ACS APPLIED MATERIALS & INTERFACES

www.acsami.org

Research Article

Photosensitive Polymeric Janus Micromotor for Enzymatic Activity Protection and Enhanced Substrate Degradation

Pedro Mena-Giraldo and Jahir Orozco*

Cite This: https://doi.org/10.1021/acsami.1c14663

Read Online

ACCESS | Metrics & More | Article Recommendations | Supporting Information

ABSTRACT: Immobilizing enzymes into microcarriers is a strategy to improve their long-term stability and reusability, hindered by (UV) light irradiation. However, in such approaches, enzyme−substrate interaction is mediated by diffusion, often at slow kinetics. In contrast, enzyme-linked self-propelled motors can accelerate this interaction, frequently mediated by the convection mechanism. This work reports on a new photosensitive polymeric Janus micromotor (JM) for UV-light protection of enzymatic activity and efficient degradation of substrates accelerated by the JMs. The JMs were assembled with UV-photosensitive modified chitosan, co-encapsulating fluorescent-labeled proteins and enzymes as models and magnetite and platinum nanoparticles for magnetic and catalytic motion. The JMs absorbed UV light, protecting the enzymatic activity and accelerating the enzyme−substrate degradation by magnetic/catalytic motion. Immobilizing proteins in photosensitive JMs is a promising strategy to improve the enzyme's stability and hasten the kinetics of substrate degradation, thereby enhancing the enzymatic process's efficiency.

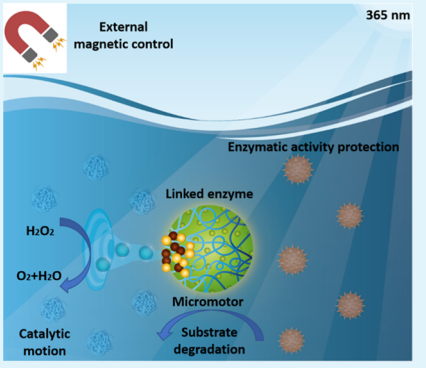

KEYWORDS: *micromotors, photosensitive microcarriers, cargo, enzymatic activity protection, accelerated substrate degradation*

Downloaded via Jahir Holgu&#65533;&#65533;n on January 3, 2022 at 13:02:13 (UTC).
See https://pubs.acs.org/sharingguidelines for options on how to legitimately share published articles.

INTRODUCTION

Micro-immobilization is a swiftly growing strategy to embed enzymes into micromaterials to protect the enzymatic activity and improve stability, substrate degradation, and reusability.[1−3] The diffusion mechanism mediates the immobilized enzyme−substrate interaction, but it is frequently achieved at slow kinetics.[4] The enzyme linked to self-propelled motors accelerates this interaction remarkably for substrate degradation, often mediated by the convection mechanism.[5] In this context, motor-coupled enzymes have been widely explored not only for powering a wide variety of micro/nanomotor structures[6−9] but also for multiple dynamic duties, including cargo transport,[10] sensing,[11] and remediation,[12] in the biomedical[13] and environmental[14] fields, for example, accelerated degradation or remotion of tetramethylbenzidine (TMB),[15−17] 2-amino-4-chlorophenol (2A4CP),[18,19] and other substrates.[20−22]

Janus micromotors (JMs) based on microcarriers with magnetic and catalytic motion have an accelerated cargo−medium interaction.[23,24] The catalytic reaction between platinum (Pt)[25] or catalase (Cat) with hydrogen peroxide (H_2O_2)—as fuel—produces oxygen bubbles on one side of the anisotropic JMs used as driving force for their motion.[26,27] JMs have been straightforwardly assembled by soft chemistry and bottom-up approaches[28] of lower cost than the top-down approach counterparts.[29] Polymeric JMs based on Mg, Pt, and Fe_3O_4 nanoparticles (NPs) and polymeric carriers such as polymeric spheres,[30] polymersomes,[31] and polymeric stomatocytes[32] have also been designed to propel by magneto/catalytic movement for cargo transport and protection[33] but not in connection to enzymatic activity protection, the main novelty of this work.

Oxidoreductases (OTs) degrade the substrate by the oxide-reduction mechanism, catalyzing oxygen insertion, hydrogen transfer, and proton extraction steps.[34] Horseradish peroxidase (HRP), laccase (Lac), and Cat enzymes are representative OTs,[35] which have been used in a myriad of applications, such as organic pollutant remediation,[35] pharmaceutical biodegradation,[36] chemical synthesis, clinical medicine, enzyme-linked immunosorbent assays (ELISAs),[37] biosensors and clinical diagnosis,[38,39] water-quality testing,[40] bioremediation, food industry,[41] and enzymatic motor propulsion.[42] However, the OTs lose their enzymatic activity by changes in the medium's ionic strength, temperature, pH, or chemical composition, hindering substrate degradation in multiple uses.[43] Some OTs such as HRP,[44] Lac,[45] and Cat[46] exhibit inactivation by UV-light exposition, limiting their use in the presence of sunlight. Functionalizing an enzyme with UV-absorbing molecules (UV-AMs) and covering it with TiO_2 NPs have shown enzymatic

Received: August 2, 2021
Accepted: December 23, 2021

© XXXX American Chemical Society

Scheme 1. (A) Schematic Illustration of Photosensitive Chitosan Polymer (PCH), Fe_3O_4, and Pt NP Synthesis, J-PCM Self-Assembly, Enzyme Immobilization, Enzymatic Activity Protection against UV Irradiation, and Dynamic Substrate Degradation Accelerated by Both Magnetic Fe_3O_4 NPs and Depletion of H_2O_2 Catalyzed by Pt NPs, Respectively; (B) SEM Micrograph in the Secondary Electron Mode of J-PCMs with Spherical Morphology and the Corresponding EDX Images of the Distribution of C, Fe, and Pt; the Scale is 5 μm

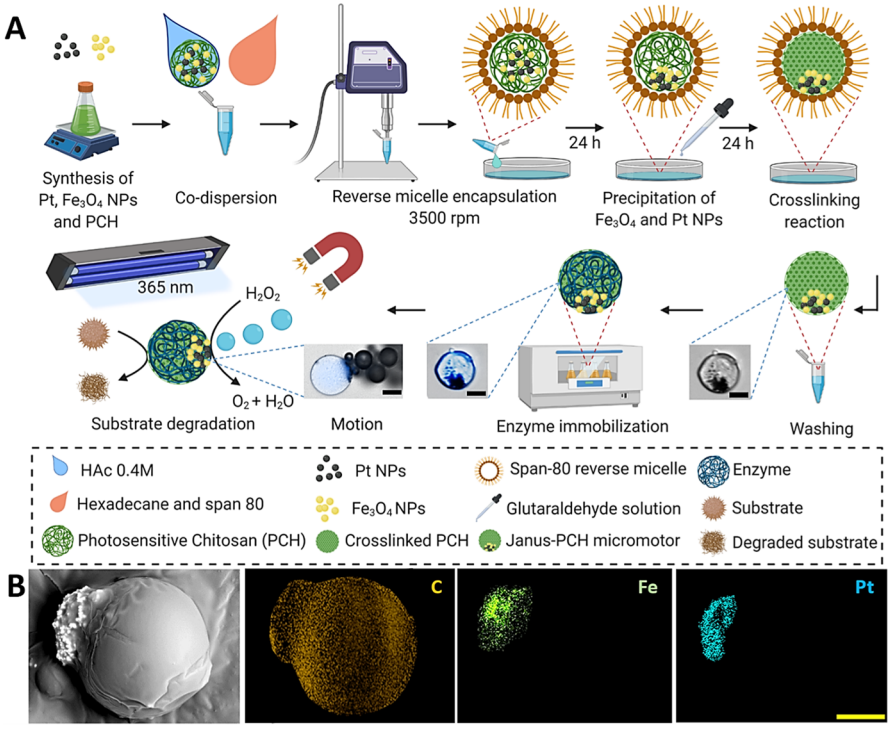

protection against UV light.[47] However, UV-AMs functionalized directly on the enzyme may compromise their stability and catalytic center availability.

Photosensitive molecules (PMs) absorb UV-light energy by the photoisomerization mechanism.[48] Conjugating PMs to polymers is a straightforward manner to assemble UV-photosensitive polymeric micro/nanocarriers (PCs) with the ability to release the cargo by UV-light stimulus, taking advantage of the high UV-light absorption of PMs for the photoactivation process.[49,50] Similarly, light-stimulated polymeric JMs are emerging approaches that use UV-light energy to generate propulsion, cargo transport, environmental control and remediation, biosensing, and cancer therapy, highlighting the importance of biophotonic on the micro/nanomotor field.[51]

We report on a new Janus UV-photosensitive polymeric chitosan micromotor (J-PCM), assembled with soft-chemistry and bottom-up technologies to demonstrate for the first time enzymatic activity protection against UV light using UV-AMs and efficient degradation of substrates accelerated by self-propelled catalytically and externally controlled magnetic field motion (Scheme 1). The novel photosensitive polymer was synthesized by covalently linking UV-photosensitive azobenzene molecules to chitosan. The J-PCMs were assembled by reverse micelles, while co-encapsulating magnetite and Pt NPs precipitated by gravity as the principle mechanism for the anisotropic micromotor formation process. DAPI and FITC proteins and HRP, Lac, and Cat enzymes were efficiently immobilized by diffusing them into the micromotor's inner side and cross-linking them with glutaraldehyde. Although the photoisomerizable azobenzene molecules demonstrated to absorb UV light protecting the enzymatic activity (Scheme 2), the J-PCM motion accelerated degradation of TMB, syringaldazine (SYR) substrates, and bioremediation of 2A4CP phenolic pollutant. The designed soft-chemistry methodology represents a new and cost-affordable approach for synthesizing micromotors compared to high-cost top-down technologies. Overall, our approach demonstrated to be a promising strategy to improve the stability of enzymes and the substrate degradation kinetics advancing the enzymatic process efficiency with potential use in enzyme-based environmental intervention and industrial catalytic processes. This is the first time an azobenzene molecule is linked to CH to synthesize a new polymer (PCH) to form microcarriers with cross-linked enzymes and the first probe of enzymatic activity protection against UV light and dynamic substrate degradation by UV-AMs and enzymes linked to moving microcarriers (Scheme 2).

EXPERIMENTAL SECTION

Synthesis of UV-Photosensitive Chitosan. The photosensitive polymer was synthesized, as shown in Scheme 2. The UV-light photoresponsive group (PhBA) was activated with DCC/NHS in 0.6 mL of methanol with a 1:2:1 PhBA/NHS/DCC molar ratio, under constant stirring for 12 h at 20 °C in the dark. Diluted chitosan (CH) solution in 0.4 M acetic acid (20 mg m^{-1}) was added over the activated PhBA (2:1 PhBA/chitosan molar mass ratio) to react for 48 h in the dark, after which the UV-PCH was obtained. PCH was precipitated with NaOH (5 wt %), filtered, and washed with acetone, methanol, and ethanol. Finally, PCH was dried at 60 °C for 6 h, macerated in a mortar to homogenize the sample, and introduced into a desiccator to remove the remaining moisture.

Synthesis of Pt and Fe_3O_4 NPs. A total of 50 mg of H_2PtCl_6 was dissolved in 1 mL of H_2O (type I) under constant stirring (1000 rpm) at 40 °C for 10 min. Hydrazine was added dropwise until the solution

https://doi.org/10.1021/acsami.1c14663
ACS Appl. Mater. Interfaces XXXX, XXX, XXX−XXX

Scheme 2. Synthesis, Enzyme Immobilization, and Photoisomerization Process of UV-Photosensitive Polymeric JMs

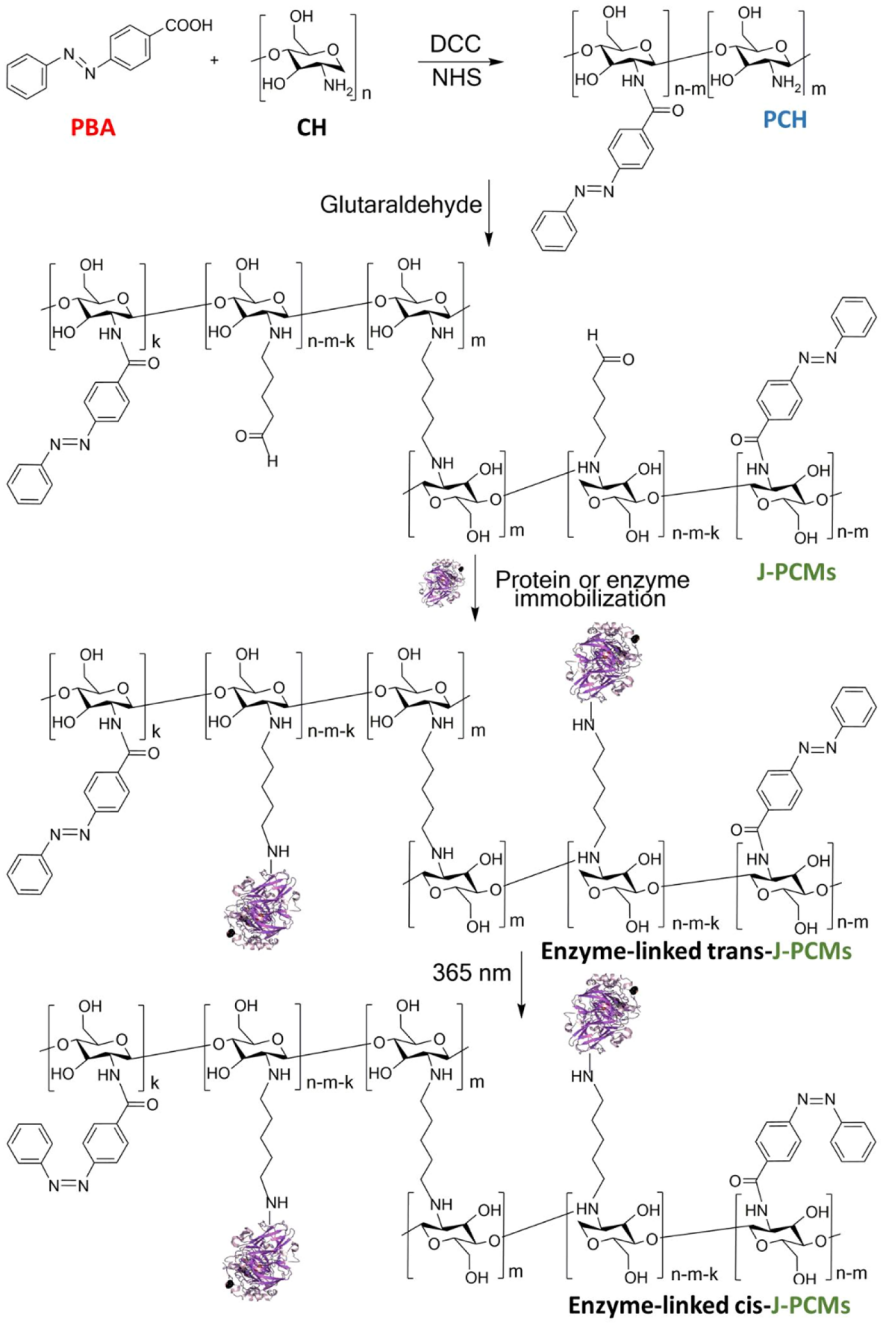

had a pH higher than 10 and stirred for 40 min under the same conditions. A black precipitate of Pt NPs was obtained with an average size of 139.3 ± 32.7 nm, washed once with water and twice with ethanol, dried under 60 °C for 2 h, and stored in hexane. 1.5 mmol (300 mg) $FeCl_2{\cdot}4H_2O$ and 2.3 mmol (611 mg) $FeCl_3{\cdot}6H_2O$ were stirred at 1000 rpm in 5 mL of deionized water at room temperature for 10 min. A total of 2 mL of 25% ammonium hydroxide solution was added dropwise over the solution and stirred for 5 min. 0.7 mmol (125 mg) citric acid was poured over the reaction mixture and heated up to 70 °C for 1 h and 110 °C for 2 h. A black precipitate of citric acid-coated Fe_3O_4 NPs was obtained with a singular average of 195.4 ± 53.1 nm and an average agglomerate size of 471.2 ± 174.1 nm, caused by the presence of citric acid, washed several times with distilled water, and dried under 60 °C overnight.

J-PCM Self-Assembly. First, 200 μL of homogeneous and aqueous dispersion of 20 mg mL^{-1} PCH, 1.5 mg of Pt, and 1.5 mg of Fe_3O_4 NPs was co-solubilized with 2% (wt) of the span 80 surfactant in 400 μL of hexadecane organic medium through an ultra-turrax homogenizer. Then, after 24 h of resting, 125 μL of 12.5% glutaraldehyde solubilized in span 80/hexadecane was dripped over PCH microdroplets. Finally, after 24 h, the J-PCMs were washed with ethanol three times and resuspended in PBS-1× to store.

Catalytic and Magnetic Motion Experiments. An inverted microscope was used for taking motion videos of J-PCMs and for their tracking analysis. A total of 2 μL of 1.5% surfactant (Triton X-100), 2 μL of 9% H_2O_2, and 2 μL of 1 mg mL^{-1} J-PCMs were put on a glass slide to get 0.5 and 3% final concentration of surfactant and H_2O_2, respectively, for the catalytic motion. A total of 2 μL of 1 mg mL^{-1} J-PCMs and 4 mL of distilled water were put on a glass slide, and a neodymium magnet was used for controlling the magnetic motion of the J-PCMs.

PB-ST and FITC-Peptide Linking to J-PCM Process. A total of 0.23 mg of J-PCMs was previously incubated in PBS 1× for 20 h to condition and enhance their linking viability in the medium. A total of

https://doi.org/10.1021/acsami.1c14663
ACS Appl. Mater. Interfaces XXXX, XXX, XXX−XXX

50 μL of PB-ST or FITC-peptide (1 mg mL^{-1}) in PBS 1× was stirred in a shaker at 800 rpm and 37 °C for 1 h and kept overnight at 4 °C. The J-PCM-linked protein was washed several times with PBS 1×, once with PBS 1×-tween, and with PBS 1× once more until the fluorophore wavelength signal in the supernatant was not detected and finally stored in PBS 1× at 4 °C.

HRP, Lac, and Cat J-PCM Linking Process. A total of 1 mL (2 mg mL^{-1}) of J-PCMs was incubated with PBS 1× for 2 h, precipitated with the magnetic field, and separated from the dispersion. Then, the precipitate was washed once with PBS 1×, resuspended with HRP, Lac, or Cat solution at 0.21 mg mL^{-1} in PBS buffer 1×, PBS buffer (pH 6.5), and PBS (pH 7.0), respectively, stirred in a shaker for 1 h at 25 °C, and subsequently allowed to stand at 4 °C for 12 h and 2 h for the HRP and Lac solutions, respectively, and 37 °C for 2 h for the Cat solution. The J-PCM-linked enzymes were washed several times with the respective buffer, once with PBS 1×-tween, and with PBS 1× once more, until enzyme activity in the supernatant was not detected, and stored in PBS 1×, PBS pH 6.5, and PBS pH 7.0 at 4 °C for HRP, Lac, and Cat, respectively.

Loading Capacity of J-PCMs. An excess of protein was incubated with the J-PCMs (previous section). After the protein immobilization process, the remaining not-linked enzyme was removed by applying the magnetic field for 5 min. The resultant free protein in the supernatant was then collected. It was proved with the disaggregation of J-PCMs in acidic solution and the quantification of the delivered enzyme.

Enzymatic Activity Protection Against UV Light. 1 mg mL^{-1} free-HRP, -Lac, and -Cat or 2 mg mL^{-1} J-PCM-linked enzyme in PBS 1×, PBS pH 6.5, and PBS pH 7.0 solutions was exposed to 365 nm UV light, from 0 to 60 min in 5 min intervals, respectively. The relative activity was determined for 12 ng mL^{-1} free-HRP, 0.15 mg mL^{-1} free-Lac and -Cat, and 330 ng mL^{-1}, 50 μg mL^{-1}, and 150 μg mL^{-1} J-PCM-linked HRP, Lac, and Cat, for each time interval, with 0.3 mM TMB, 0.041 mM SYR, and 1.41 mM TMB, respectively. The quantification was made by UV spectrophotometry, following the maximum intensity at 650 nm for TMB and 530 nm for SYR.

TMB (HRP), SYR (Lac), 2A4CP (Lac), and TMB (Cat) Degradation Experiments. A total of 2 mL of 0.3 mM TMB, 0.041 mM SYR, 6.25 μM 2A4CP, and 1.41 mM TMB were added into Petri dishes as the base solutions, respectively. 2 mg mL^{-1} (978×10^3 J-PCMs mL^{-1}) J-PCM-linked HRP, 4 mg mL^{-1} (1956×10^3 J-PCMs mL^{-1}) J-PCM-linked-Lac and -Cat, and free enzymes (equivalent concentration of immobilized enzymes) were used for the degradation process in four Petri dishes with the mentioned conditions, and their respective controls, that is, for dynamic J-PCM-linked-HRP and -Lac experiments; magnetic and static J-PCM-linked Cat (without Pt NPs) in the presence of H_2O_2, catalytic J-PCM, and magnetic J-PCM-linked Cat for Cat experiments; and free enzyme, UV light, static J-PCM-linked enzyme, and dynamic J-PCMs for HRP, Lac and Cat experiments. The magnetic movement was controlled with an external magnetic field at 800 rpm. All of them were exposed to UV light at 365 nm.

Reusability Cycles of the J-PCM-Linked Enzyme. The relative activity of J-PCM-linked HRP, Lac, and Cat (2, 4 and 4 mg mL^{-1}, respectively) was determined in a microcentrifuge tube with 1 mL of 0.3 mM TMB, 0.041 mM SYR, and 1.41 mM TMB, respectively. After the first TMB degradation, the J-PCM-linked HRP, Lac, and Cat were washed thrice with PBS 1×, PBS pH 6.5, and PBS pH 7.0, once with tween-PBS 1×, and once again with PBS pH 6.5 and PBS pH 7.0, respectively. The residual activity was calculated with 0.3 mM TMB, 0.041 mM SYR, and 1.41 mM TMB, respectively, and so on, consecutively.

Enzymatic Activity Behavior in the Presence of H_2O_2. Enzymatic activity was determined with TMB (HRP), SYR (Lac), and TMB (Cat) degradation experiments. It was tested with 0 and 3% H_2O_2, quantifying the substrate degradation with the absorbance methodology in a 96-well plate, using the Varioskan previously described, with 800 rpm stirring condition, to not have a diffusion restriction in the substrate degradation by the enzymes.

For UV-photosensitive chitosan microcarrier (PCMC) self-assembly, characterization of chemical structures and detailed spectral data of PCH and PCMC synthetic routes for ^{1}H NMR and Fourier transform infrared spectroscopy (FT-IR), quantification of free primary amines of CH and PCH, morphological, microstructural, and fluorescence microscopy and spectrophotometry characterization, J-PCM photoisomerization degree, UV-light exposure, and tracking of the J-PCM trajectories for velocity quantification upon a time, please refer to the Supporting Information section. For loading capacity of J-PCM quantification, concentration and fluorescence protection of FITC peptide and PB-ST in J-PCMs, the concentration of HRP, Lac, and Cat in J-PCMs, UV-light effect over the FITC peptide and J-PCM-linked PB-ST, K_m and V_{max} determination, TMB (HRP), SYR (Lac), 2A4CP (Lac), and TMB (Cat) degradation quantification, and supporting videos and velocity quantification, also see the Supporting Information section.

Scheme 1 illustrates the methodology for synthesizing and self-assembling J-PCMs, protein immobilization, enzymatic activity protection against UV light, and kinetic-accelerated substrate degradation employing H_2O_2 depletion from Pt NPs for catalytic and Fe_3O_4 NPs for magnetic motion, respectively. Scheme 2 displays the photosensitive chitosan polymer (PCH) and J-PCM synthesis, enzyme immobilization, and photoisomerization mechanisms from UV-light absorption.

RESULTS AND DISCUSSION

PCH synthesis consists of an amidation reaction between a carboxyl terminal azobenzene PM as UV-AMs with amine groups from chitosan by covalent linking, leading to a high and controlled distribution of the UV-AMs into the chitosan polymer backbone (Scheme 2). Pt and Fe_3O_4 NPs were synthesized using the reduction[52] and nanoprecipitation[53] methods, respectively (Figure S1, Supporting Information). A soft-chemistry process was used to form J-PCMs as a new strategy to simplify current methodologies and facilitate replication (Scheme 1). An aqueous dispersion of PCH, Pt, and Fe_3O_4 NPs was co-dispersed and homogenized by high energy to produce inverse micelles in an organic solvent with the aqueous dispersion encapsulated in the core. The inverse micelles behave template-like due to organic solvent viscosity. Gravity action precipitated the NPs in one of their sides after 24 h of resting. Glutaraldehyde solubilized in a surfactant/organic solvent dripped over PCH microdroplets started a cross-linking reaction between PCH free amines[54] and gelled the PCH polymer with NPs entrapped in one side, allowing to form the anisotropic J-PMCs. Washing with ethanol and removing the organic solvent excess and the inverse micro-emulsions left free the aldehydes and amines in the solid−gel micromotors for protein immobilization. The J-PCMs have three different motion types, magnetic due to the presence of magnetite, catalytic from the oxygen bubbles ejected from one J-PCM side by Pt-catalyzed depletion of the H_2O_2, and magnetocatalytic using both combined (Scheme 1A). SEM micrographs show the anisotropic characteristic of the spherical J-PCMs checked with EDX images with C, Fe, and Pt distribution as expected and the diameter size of 12 μm (Scheme 1B) and the secondary electron (SEI) and back-scattered (BES) modes for NP differentiation into J-PCMs (Figure S2A,B, Supporting Information, respectively). Although chitosan JMs have been developed with the inverse micelle method and a cross-linking strategy with a microfluidic system,[23] this work is the first attempt to simplify the process using gravity to produce anisotropic microcarriers, employing merely a homogenizer for microdroplet formation.

https://doi.org/10.1021/acsami.1c14663
ACS Appl. Mater. Interfaces XXXX, XXX, XXX−XXX

PCMC and J-PCM synthesis consists of the cross-linking of free amines from both the PCH and the protein with glutaraldehyde for the immobilization and homogeneous distribution of azobenzene in the microcarriers. As a result, the azobenzene segments can photoisomerize by UV-light exposition and, consequently, absorb the UV energy, acting like a homogeneous protecting barrier (Scheme 2). UV-AMs have been linked to chitosan and their derivatives, which absorb the UV energy for cargo delivery,[55,56] sunscreen development,[57] photosensitizer viability,[58] and cell attachment control[59] strategies. However, to the best of our knowledge, this is the first time that an azobenzene molecule was linked to CH to synthesize a new polymer (PCH) with the ability to form microcarriers with attached cross-linked enzymes. It is also important to remark that this is the first probe of enzymatic activity protection against UV light and dynamic substrate degradation by UV-AMs and enzymes linked to moving microcarriers (Scheme 2).

The PCH and PCMC synthesis was characterized by FT-IR and proton nuclear magnetic resonance (^{1}H NMR) (Figures 1A and S3, Supporting Information). Figure 1A shows the FT-IR spectrum of the PCH (blue line) from chitosan (CH, black line) and 4-phenylazobenzoic acid (PBA, red line). The formation of the amide at 3325 cm^{-1} (linked group) and the fact that the carbonyl from the PBA carboxylic group at 1680 cm^{-1} disappears in the PCH evidenced that the synthesis processes of the photosensitive polymer occurred. The −OH vibration (3404 cm^{-1}) is more sensitive than the −NH$_2$ stretching band (not evidenced) in the CH spectrum. In this context, the characterization of primary amines was achieved with the stretching vibration among scissoring absorptions from 1578 to 1662 cm^{-1}. However, when the secondary amide from PCH was formed, the bending vibration band at 3325 cm^{-1} appeared, and the −OH vibration at 3474 cm^{-1} was maintained due to low reaction efficiency, which is essential to have free −NH$_2$ groups. The permanence of the signal at 1574 cm^{-1} (from CH in PCH) confirms the presence of primary amines, necessary for further microcarrier self-assembling through the cross-linking reaction.

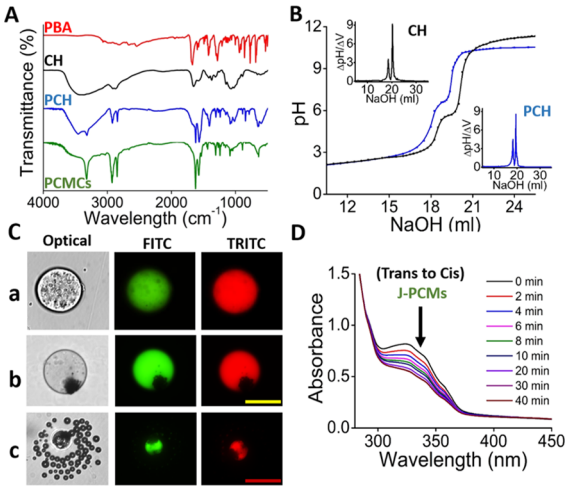

Figure 1. Characterization of the polymer precursor and J-PCMs. (A) Characterization of the PCMC synthetic route by FT-IR. (B) Potentiometric titration of CH (black line) and PCH (blue line) and the corresponding second derivative to determine the inflection points (black and blue graphic insets, respectively). (C) Fluorescence microscopy images of the self-fluorescent photosensitive chitosan, the J-PCMs, and the Pt and Fe_3O_4 NPs (observed with the optical, FITC, and TRITC filters, at 600 ms of UV-exposition time), respectively. Synthesis and formation of the PCMCs (a) and development (b) and self-propulsion (c) of the J-PCMs. (D) UV−vis spectra variation of J-PCMs induced by photoisomerization at different UV-exposure times. The scale bars are 12 μm (yellow) and 25 μm (red), respectively.

The presence of principle signals of PBA and CH ^{1}H NMR spectra (Figure S3A,B, Supporting Information, respectively) and the PCH ^{1}H NMR spectrum (Figure S3C, Supporting Information) confirmed the PCH synthesis. The PCH ^{1}H NMR spectrum was characterized by 8.19−7.62 ppm signals from the azobenzene rings, (Figure S3Ca, Supporting Information, respectively), 3.47−3.40 ppm signals from the CH ring (Figure S3Cc, Supporting Information), 3.28 ppm signal from CH-available amine, and 1.72 ppm from acetylation of CH (Figure S3Cc−e, Supporting Information, respectively). The addition reaction between PBA and CH for PCH synthesis was evidenced through PCH FT-IR and ^{1}H NMR spectra, which characterized the produced amide and PBA in the CH polymer. Therefore, it was necessary to estimate the extent of free amine groups from PCH (Table S1, Supporting Information) to evaluate the PCH capabilities to cross-link with glutaraldehyde and then to form the PCMCs and J-PCMs, by potentiometric titration (65.1%) (Figure 1B) and FT-IR (67.1%) (Figure S3E, Supporting Information), using eqs S1 and S2 (Supporting Information), respectively. Then, the extent of azobenzene molecules introduced into the CH backbone was 16% from eq S3. The FT-IR characterization shows the spectrum of PCMCs corresponding to the J-PCMs (Figure 1A-PCMCs). The main functional groups present a band extension at 3326 and 1626 cm^{-1}, which confirmed the Schiff's base formation by the cross-linking reaction between the free amines and aldehyde groups.[60] Optical and fluorescence micrographs of J-PCMs show their spherical morphology and anisotropic and self-fluorescence characteristics observed with optical, FITC, and TRITC filters at a high UV-light exposure time (Figure 1C). CH-glutaraldehyde cross-linking interaction allows observation of the low self-fluorescence of the J-PCMs in green and red color emissions.[61,62] Dark spots in J-PCM micrographs evidence the Fe_3O_4 and Pt NPs compared to PCMCs (Figure 1Ca), showing their anisotropic characteristic (Figure 1Cb). Oxygen bubbles from Figure 1Cc evidenced the J-PCM self-propelling characteristics after the catalysis reaction between the Pt NPs and H_2O_2 (3%) in an aqueous medium. Azobenzene compounds generally do not present self-fluorescence[63] because they do not emit light after UV-light exposure but absorb it through trans−cis photoisomerization effect, succeeding excitation to the S_1 ($n \rightarrow \pi^*$) state around the N═N double bond.[64] However, when the azobenzene is within a compact structure, it is possible to evidence blue[65] and low-green[66] self-fluorescence, which is not evidenced by fluorescence emission detection. The J-PCM UV-light absorption was studied through the evolution of the UV−vis transition bands from the azobenzene units upon a time by following the signal decrease at 331 nm. Thus, after 30 min of UV-light exposure, the J-PCMs experienced the maximum photostimulation extent (Figure S4, Supporting Information) because the contained azobenzene absorbed the UV irradiation up to 30 min (Figure 1D).

From a representative sample of J-PCMs (Figure 2A-left), the average diameter was estimated to be 12.5 ± 1.3 μm (n = 12) calculated through the normal distribution of each particle

https://doi.org/10.1021/acsami.1c14663
ACS Appl. Mater. Interfaces XXXX, XXX, XXX−XXX

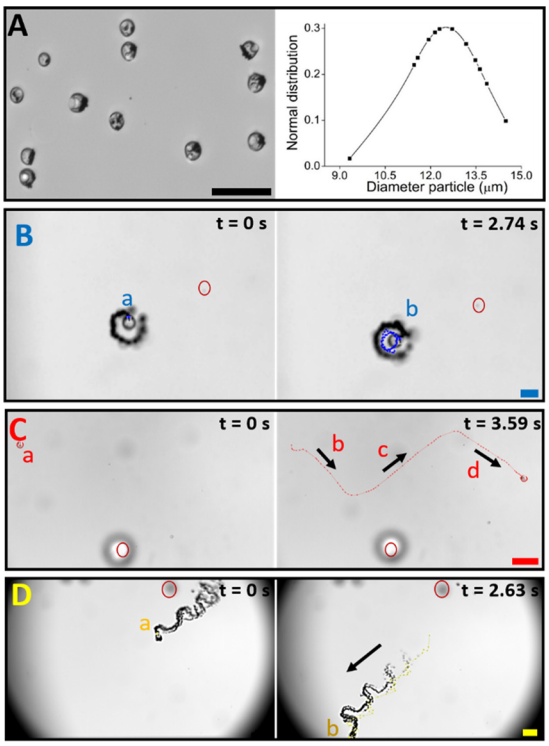

Figure 2. Characterization of micromotor movement. (A) Optical microscopy image of the J-PCMs (left) and the corresponding normal distribution of their particle size (right). Tracking of the dynamic movement of J-PCMs. (B) Catalytic movement for 0 s (left) and 2.74 s (right). (C) Magnetic movement for 0 s (left) and 3.59 s (right). (D) Magnetocatalytic movement for 0 s (left) and 2.63 s (right). Data come from Videos S1, S4, and S6, from the Supporting Information, respectively. The black, blue, red, and yellow scale bars are 20, 25, 50, and 100 μm, respectively.

diameter (Figure 2A-right). The catalytic movement of J-PCMs was characterized by the tracking software from the Nikon microscope, whose average velocity was 198.3 ± 12.6 μm s^{-1} (15.9 body lengths s^{-1}) (n = 10) in a 3% H_2O_2 aqueous solution containing 3% surfactant (Figures 2B and S5A). Please see single catalytic (but no magnetic) (Video S1), zoomed-in JPCM (Video S2), and multiple motion (Video S3) in the Supporting Information. Similarly, the J-PCMs displayed magnetic movement with three and four linear trajectories in different directions with an average velocity of 45.5 ± 10.3 μm s^{-1} (3.6 body lengths s^{-1}) (Figures 2C and S5B), by optical (Video S4) and fluorescence imaging (Video S5) in the Supporting Information, respectively, in which their self-fluorescence can be used for tracking. Interestingly, J-PCMs showed magneto-catalytic movement with a propelling/motion in multiple directions and one orientation to interact with the medium at an enhanced velocity of 600.4 ± 35.4 μm s^{-1} (48.0 body lengths s^{-1}) (Figures 2D and S5C and Video S6 in the Supporting Information). The J-PCM motion will have a profound impact on the enzyme−substrate accelerated interaction kinetics, as demonstrated below. Furthermore, magnetic guidance of self-propelled J-PCMs permits their proper external control for advanced applications, such as site-specific substrate degradation,[67] removal of J-PCMs for enzymatic activity reactivation and reusability,[68,69] and biosensing[70] and assessing the level of cellular interaction,[71] among others.

The spherical morphology, diameter size, and cross-linking of CH with glutaraldehyde of J-PCMs allow high surface and support area[72] available for protein linking. The J-PCMs based on the CH biopolymer provide hydrophilicity, biodegradability,[73] and biocompatibility.[74] The J-PCM protein immobilization ability was demonstrated by loading an FITC peptide and PB-ST, covalent immobilization, and absorption interaction and taking advantage of the available primary amines from the peptide and C−C affinity, respectively. Fluorescence micrographs show the green and blue color emissions of the model proteins immobilized on the J-PCMs (Figure 3Aa,b) and their respective CH JM control (without chromophore) (Figure 3Ac,d) compared by optical, FITC, and DAPI filters, and the three of them merged (Figure S6, Supporting Information). FITC peptide and PB-ST loading capacity were determined (Table S3, Supporting Information), employing eqs S4 and S5, (Supporting Information), showing higher loading capacity of the covalent immobilization methodology with respect to the absorption one counterpart. The J-PCMs absorb the UV irradiation protecting the fluorescence capacity of the conjugated protein, which were quantified by RFU spectra to be around 97 and 70% for FITC peptide- and PB-ST-linked J-PCMs, respectively, after 30 min of UV exposure (Figure 3B), compared to 50% FITC peptide- and 40% PB-ST-linked J-CMs, respectively, used as the control (Figure S7 and Table S4, Supporting Information). Fluorescence protection by UV-AMs present in the J-PCMs was evidenced due to the initial fluorescence of the protein linked to the J-PCMs kept constant (stable) upon UV irradiation. The high loading (immobilization) efficiency comes from free amine groups available in the protein. The protein-fluorescence protection against UV-light irradiation opened up opportunities to extend fluorescence intensity and protein activity upon time for encapsulated protein-based applications.

HRP, Lac, and Cat were covalently linked to J-PCMs through the free amines from the enzymes, the enzyme-loading capacity (Table S3, Supporting Information), and the Michaelis−Menten constants of J-PCM-linked enzymes concerning the free enzymes were assessed (Table S5, Supporting Information), utilizing eq S6−S18 (Supporting Information), based on Figures S8 and S9 (Supporting Information), respectively. K_m and V_{max} constants displayed a similar behavior when comparing the enzyme-linked J-PCMs and free enzymes, having a relatively low restriction in the substrate diffusion to the linked enzyme thanks to the J-PCM gel-like absorption property from chitosan and the cross-linking methodology used. Thus, the catalytic center of the linked enzyme has high availability for substrate interaction and further degradation. Furthermore, a magnetic J-PCM enzyme-based platform allows the enzyme activity reactivation and reuse, compared to free-enzyme applications of a single use, showing reusability of 2, 6, and 2 cycles with 80% of enzymatic activity extent for HRP-, Lac-, and Cat-linked J-PCMs, respectively (Figure S10, Supporting Information). The J-PCM magnetic properties extend the shelf-life of immobilized proteins, allowing a high control for dynamic degradation, extraction, and reuse.

Enzymatic UV-photoinactivation assay compared the enzymatic activity from the enzyme-linked to J-PCMs versus the free enzyme following the evolution of the UV−vis transition bands from the corresponding substrate upon a time (Figure 3C). Although relative activity of the HRP and Lac immobilized into the J-PCMs was protected 100 and 85%,

https://doi.org/10.1021/acsami.1c14663
ACS Appl. Mater. Interfaces XXXX, XXX, XXX−XXX

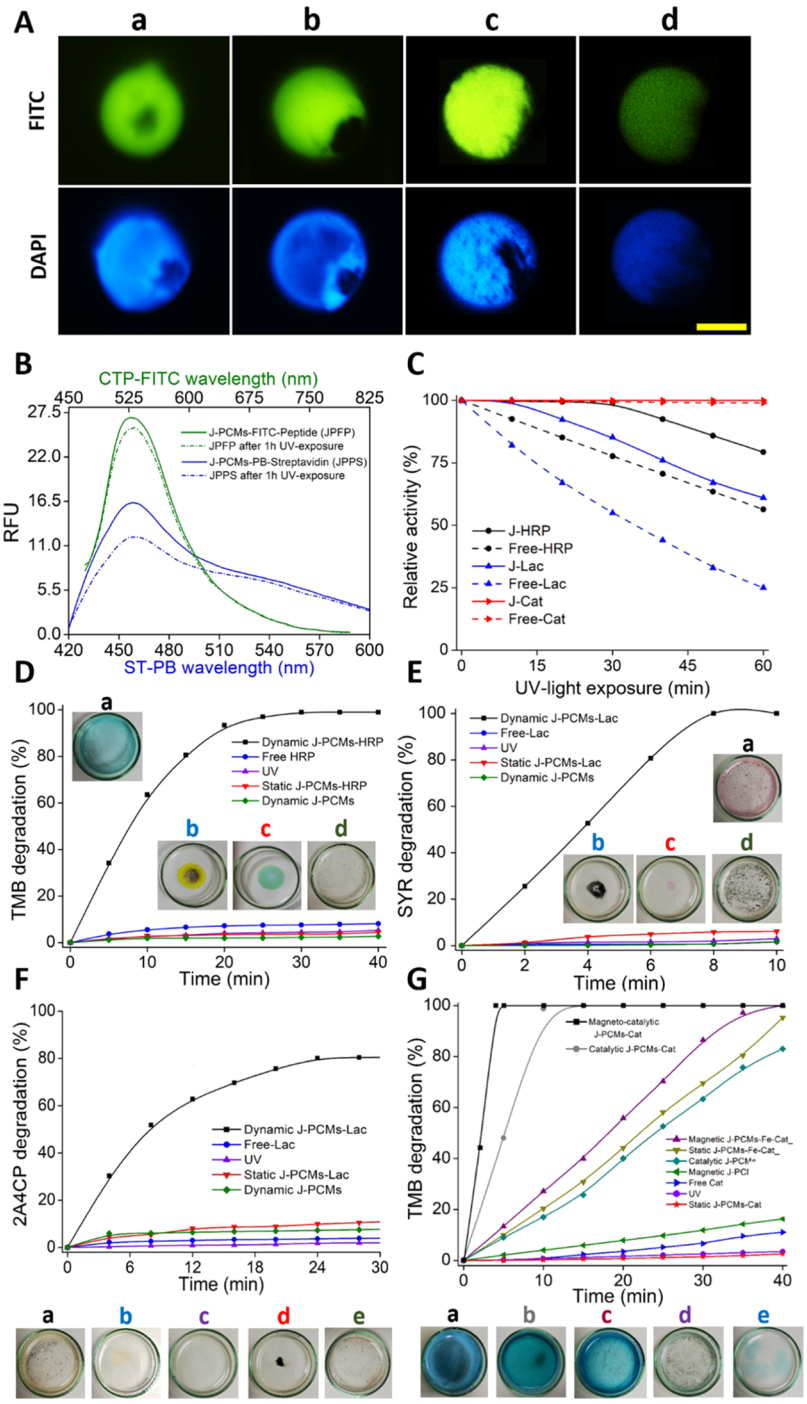

Figure 3. Enzymatic protection and enhanced substrate degradation. (A) Fluorescence microscopy images of the J-PCMs (a,b) and J-CMs (control) (c,d) loaded with FITC peptide and PB-ST, before (a,c) and after 30 min UV exposure (b,d), observed by the FITC and DAPI filter, at 71 and 50 ms of UV-exposition time, for the FITC peptide and PB-ST, respectively. The scale bar is 6 μm. (B) Fluorescence of FITC peptide (green graphic) and PB-ST (blue graphic) loaded at the J-PCMs: RFU spectra before (continuous line) and after 30 min UV-light exposure (dotted line). (C) Relative activity under UV-light exposure. (D) TMB degradation under UV-light exposure. Pictures of TMB degraded after 25 min of reaction for the dynamic J-PCM-HRP (a), free HRP (b), static J-PCM-HRP (c), and dynamic J-PCMs (d). (E) SYR degradation under UV-light exposure. Pictures of SYR-degraded after 10 min of reaction for the dynamic J-PCM-Lac (a), static J-PCM-Lac (b), free Lac (c), and dynamic J-PCMs (d). (F) 2A4CP degradation under UV-light exposure. Pictures of 2A4CP-degraded after 30 min of reaction for the dynamic J-PCM-Lac (a), free Lac (b), UV-light (c), static J-PCM-Lac (d), and dynamic J-PCMs (e). (G) TMB degradation under UV-light exposure. Pictures of TMB-degraded after 40 min of reaction for the magneto-catalytic J-PCM-Cat (a), catalytic J-PCM-Cat (b), magnetic J-PCM-Cat (c), dynamic J-PCMs (d), and free Cat (e).

respectively, for 30 min, the one of Cat-linked and free Cat was 100% upon UV exposure even for 60 min. The free-HRP and -Lac underwent 23 and 54% decreased relative activity after 30 min of UV-light exposure, while Cat's activity remained unchanged (Figure 3C). UV-irradiation photoinactivated the HRP and Lac enzymatic activity, preventing the proper

https://doi.org/10.1021/acsami.1c14663
ACS Appl. Mater. Interfaces XXXX, XXX, XXX−XXX

substrate oxide-reduction processes. It may be related to the heme prosthetic group of the HRP absorbing the UV light, causing photoionization,[44] and the UV-light absorption of Lac generates reactive oxygen species and singlet oxygen, thus triggering the photo-oxidation mechanisms in its amino acid residues.[45] Cat does not present photoinactivation with UV light exposure. Although 150−450 W UV-light irradiation power has been demonstrated to produce partial heme destruction and the Cat photoinactivation, this high irradiation power significantly exceeds the one used in this study (6 W).[75] The J-PCMs protected the enzymatic activity of the linked enzyme around 30 min of UV irradiation because the contained azobenzene molecule absorbs 77% of the UV energy for its trans−cis photoisomerization (Figures 1D and 3C, eq S19, Supporting Information). The 33% of UV-overlapped energy (eq S20, Supporting Information) inactivated the 15% of the Lac-linked J-PCMs in the photoisomerization time, but not the HRP counterpart because the Lac enzyme is more sensitive to UV light, demonstrating high promise for enzymatic activity protection strategies. Once this time is overpassed, unlike the J-PCMs, the enzyme adsorbs the UV irradiation truncating the protective effect as observed.

Substrate degradation assays showed accelerated and efficient kinetics by the dynamic interaction between the J-PCM-linked enzyme and the substrate (Figure 3D−F). The extent of substrate degradation was quantified using eqs S9−S11 and S21 (Supporting Information), for TMB (HRP), SYR (Lac), TMB (Cat), and 2A4CP (Lac), from Figures S8D, S8F, S8I, and S8G (Supporting Information), respectively. As H_2O_2 decreases the Lac activity (Figure S11A, Supporting Information), 100% TMB degradation was highly accelerated by an external magnetic field without H_2O_2, in 25 min reaction time with the dynamic J-PCM-HRP process, under UV exposure, compared to around 8% TMB degradation of the free-HRP, static J-PCM-linked HRP, dynamic J-PCMs, and UV light used as controls (Figure 3D). 100% SYR and 80% 2A4CP degradation under UV exposure was highly accelerated up to 10 and 30 min of degradation time with the dynamic J-PCMs-Lac process by magnetic motion, respectively, without H_2O_2 to avoid the Lac inactivation (Figure S11B, Supporting Information). Compared to approximately 7% SYR- and 10% 2A4CP of the free-Lac, static J-PCMs-Lac, dynamic J-PCMs, and UV-light controls (Figure 3E,F, respectively), the accelerated degradation by dynamic J-PCM-enzyme was within the enzymatic activity protection time (30 min) against UV light, demonstrating the enzyme's capacity for the enhanced substrate-degradation kinetics and enzyme protection against UV irradiation. The controls confirm the inefficiency of the substrate degradation processes, proving a few contributions of the UV-light-Fe_3O_4 NPs[76] and UV-light−substrate[77] interaction, like poor self-mobility of the free enzyme and low diffusion of the substrate through the medium to interact with the J-PCM-linked enzyme. In this regard, the degradation concept was tested with substrates with different enzyme affinities and 2A4CP, highlighting the potential for environmental intervention and pollutant remediation triggered by sunlight.

100% TMB degradation under UV exposure was highly accelerated in 5 min reaction time by magnetocatalytic movement, 15 min by catalytic, and 40 min by magnetic (without Pt NPs) J-PCM-Cat motion as compared to the TMB-degradation extent of 95% by static (without PT NPs) J-PCM-Lac, 81% by catalytic (without Cat) J-PCMs, 17% by magnetic J-PCM-Cat, 10% by free-Cat, 3% by UV light, and 3% by static J-PCM-Cat in 40 min of the reaction used as controls (Figure 3G). Although H_2O_2 increases the Cat activity[78] (Figure S11C, Supporting Information), it was proved that the substrate-degradation kinetics was highly accelerated with magnetocatalytic and catalytic motion, compared to the J-PCM-Cat magnetic motion control without Pt NPs and H_2O_2, when the Cat-H_2O_2 dynamic contribution was evaluated. Similarly, the Pt and Fe_3O_4 NP−H_2O_2 interaction was evaluated with the catalytic (without Cat) J-PCM control to estimate the contribution of O_2 bubbles and the Fe_3O_4 NP-UV-light synergy in the dynamic TMB degradation. Magnetic J-PCM-Cat assay proved the Cat activation because the dynamic TMB degradation was less efficient without H_2O_2. The free-Cat had more mobility in the medium than the HRP and Lac, but the diffusion was insufficient to degrade TMB efficiently. Like the other linked HRP and Lac enzymes, the UV light and substrate interaction and the static-linked Cat were evaluated as controls, showing a low TMB degradation and a diffusion restriction. Furthermore, the Cat activity was not affected by the complete photoisomerization of the azobenzene molecule into J-PCMs, allowing the proper degradation of the substrate after 30 min.

CONCLUSIONS

New UV-photosensitive polymeric JMs were synthesized and characterized through FT-IR and 1H NMR. Enzymes were linked to the J-PCMs by cross-linking with glutaraldehyde. The azobenzene present in the J-PCMs photoisomerized in 30 min UV-light absorption. J-PCMs had a spherical morphology with 12 μm of size and 600.4 μm s^{-1} of velocity in 3% H_2O_2 when propelled by the magnetocatalytic reaction. Protein immobilization and fluorescence protection concepts were demonstrated by comparing fluorescence microscopy images of J-PCMs and CH JMs without chromophores and quantifying by RFU spectra. The relative enzymatic activity of HRP and Lac immobilized into J-PCMs was protected against UV exposure compared with the free-HRP and free-Lac, respectively. TMB, SYR, and 2A4CP, as substrates of the HRP and Lac, were degraded under UV exposure by HRP- and Lac-linked J-PCMs with magnetic motion after 25, 10, and 30 min of reaction time, respectively. Free-HRP and -Lac with convection restriction, static HRP- and Lac-linked J-PCMs, dynamic J-PCMs, and UV light were inefficient in degrading TMB, SYR, and 2A4CP, as expected. Immobilized Cat into J-PCMs with magneto/catalytic motion degraded TMB with accelerated kinetics in only 5 min. Overall, the new strategy developed for enzymatic activity protection against UV light and the fast substrate degradation that impart the J-PCMs by magnetic and catalytic motion interaction improved the enzymatic activity efficiency, holding the potential to be implemented for accelerated water remediation stimulated by sunlight. Therefore, the enzyme protection and dynamically enhanced substrate degradation of the J-PCM concept could be extended to many other applications, including chemical synthesis, organic pollutant (bio)remediation, pharmaceutical biodegradation, ELISAs, biosensors, clinical medicine, and industrial applications.

ASSOCIATED CONTENT

Supporting Information

The Supporting Information is available free of charge at https://pubs.acs.org/doi/10.1021/acsami.1c14663.

https://doi.org/10.1021/acsami.1c14663
ACS Appl. Mater. Interfaces XXXX, XXX, XXX−XXX

Chemicals, experimental details, equipment, equations, tables, and additional figures (PDF)
Trajectories and scenarios depicted in Figure 2B−D in the main text and their velocity quantification from Figure S5A−C for J-PCMs catalytic, magnetic, and magneto-catalytic motions, respectively. J-PCMs catalytic motion, Video S1 (MP4)
Zoomed-in JPCM motion, Video S2 (MP4)
Multiple motion, Video S3 (MP4)
J-PCMs displayed magnetic movement with three linear trajectories in different directions by optical imaging, Video S4 (MP4)
J-PCMs displayed magnetic movement with four linear trajectories in different directions by fluorescence imaging, Video S5 (MP4)
J-PCMs showed magneto-catalytic movement in multiple directions, Video S6 (MP4)

AUTHOR INFORMATION

Corresponding Author

Jahir Orozco − *Max Planck Tandem Group in Nanobioengineering, Faculty of Natural and Exact Sciences, University of Antioquia, Medellín 050010, Colombia;* orcid.org/0000-0001-6249-8092; Email: grupotandem.nanobioe@udea.edu.co

Author

Pedro Mena-Giraldo − *Max Planck Tandem Group in Nanobioengineering, Faculty of Natural and Exact Sciences, University of Antioquia, Medellín 050010, Colombia;* orcid.org/0000-0002-4968-7902

Complete contact information is available at: https://pubs.acs.org/10.1021/acsami.1c14663

Author Contributions

P.M.-G. and J.O. conceived and designed the research. P.M.-G. carried out the experiments with the supervision of J.O. P.M.-G. and J.O. wrote the manuscript. P. M.-G. designed and drew the figures. Both authors have reviewed and approved the final version of the manuscript.

Funding

Financial support from the University of Antioquia and the Max Planck Society through the Cooperation agreement 566-1, 2014.

Notes

The authors declare no competing financial interest.

ACKNOWLEDGMENTS

P.M.-G. and J.O. acknowledge financial support from the University of Antioquia and the Max Planck Society and The Ruta N complex and EPM for hosting the Max Planck Tandem Groups. The authors acknowledge Yeison Monsalve-García for technical support.

ABBREVIATIONS

UV, ultraviolet
JMs, Janus micromotors
Pt, platinum
NPs, nanoparticles
H_2O_2, hydrogen peroxide
OTs, oxidoreductases
HRP, horseradish peroxidase
Lac, laccase
Cat, catalase
ELISAs, enzyme-linked immunosorbent assays
AMs, absorbing molecules
PMs, photosensitive molecules
PCs, polymeric micro/nanocarriers
J-PCM, Janus UV-photosensitive polymeric chitosan micromotor
TMB, tetramethylbenzidine
SYR, syringaldazine
2A4CP, 2-amino-4-chlorophenol
PCH, photosensitive chitosan polymer
SEI, secondary electron
BES, backscattered
PCMCs, photosensitive chitosan microcarriers
PBA, 4-(phenylazo)benzoic acid
NHS, *N*-hydroxysuccinimide
DCC, *N*,*N*′-dicyclohexylcarbodiimide
NaOH, sodium hydroxide
KBr, potassium bromide
DMSO, dimethyl sulfoxide
CH, chitosan
SEM, scanning electron microscopy
FT-IR, Fourier transform infrared spectroscopy
NMR, nuclear magnetic resonance

REFERENCES

(1) Ma, X.; Jannasch, A.; Albrecht, U.-R.; Hahn, K.; Miguel-López, A.; Schäffer, E.; Sánchez, S. Enzyme-Powered Hollow Mesoporous Janus Nanomotors. *Nano Lett.* **2015**, *15*, 7043−7050.
(2) Wang, L.; Hortelão, A. C.; Huang, X.; Sánchez, S. Lipase-Powered Mesoporous Silica Nanomotors for Triglyceride Degradation. *Angew. Chem., Int. Ed.* **2019**, *58*, 7992−7996.
(3) Zdarta, J.; Meyer, A. S.; Jesionowski, T.; Pinelo, M. Developments in Support Materials for Immobilization of Oxidoreductases: A Comprehensive Review. *Adv. Colloid Interface Sci.* **2018**, *258*, 1−20.
(4) Carlin, g. m.; Seenuvasan, M.; Kumar, K. S.; Kumar, A.; Parthiban, R. Review on Surface Modification of Nanocarriers to Overcome Diffusion Limitations: An Enzyme Immobilization Aspect. *Biochem. Eng. J.* **2020**, *158*, 107574.
(5) Ma, X.; Hortelão, A. C.; Patiño, T.; Sánchez, S. Enzyme Catalysis to Power Micro/Nanomachines. *ACS Nano* **2016**, *10*, 9111−9122.
(6) Arqué, X.; Romero-Rivera, A.; Feixas, F.; Patiño, T.; Osuna, S.; Sánchez, S. Intrinsic Enzymatic Properties Modulate the Self-Propulsion of Micromotors. *Nat. Commun.* **2019**, *10*, 2826.
(7) Hortelão, A. C.; Patiño, T.; Perez-Jiménez, A.; Blanco, À.; Sánchez, S. Enzyme-powered Nanobots Enhance Anticancer Drug Delivery. *Adv. Funct. Mater.* **2018**, *28*, 1705086.
(8) Xu, D.; Hu, J.; Pan, X.; Sánchez, S.; Yan, X.; Ma, X. Enzyme-Powered Liquid Metal Nanobots Endowed with Multiple Biomedical Functions. *ACS Nano* **2021**, *15*, 11543−11554.
(9) Yang, Y.; Arqué, X.; Patiño, T.; Guillerm, V.; Blersch, P.-R.; Pérez-Carvajal, J.; Imaz, I.; Maspoch, D.; Sánchez, S. Enzyme-Powered Porous Micromotors Built from a Hierarchical Micro-and Mesoporous UiO-Type Metal−Organic Framework. *J. Am. Chem. Soc.* **2020**, *142*, 20962−20967.
(10) Llopis-Lorente, A.; García-Fernández, A.; Murillo-Cremaes, N.; Hortelão, A. C.; Patiño, T.; Villalonga, R.; Sancenón, F.; Martínez-Máñez, R.; Sánchez, S. Enzyme-Powered Gated Mesoporous Silica Nanomotors for on-Command Intracellular Payload Delivery. *ACS Nano* **2019**, *13*, 12171−12183.
(11) Sentic, M.; Arbault, S.; Goudeau, B.; Manojlovic, D.; Kuhn, A.; Bouffier, L.; Sojic, N. Electrochemiluminescent Swimmers for Dynamic Enzymatic Sensing. *Chem. Commun.* **2014**, *50*, 10202−10205.

(12) Bayraktaroğlu, M.; Jurado-Sánchez, B.; Uygun, M. Peroxidase Driven Micromotors for Dynamic Bioremediation. *J. Hazard. Mater.* **2021**, *418*, 126268.
(13) Vilela, D.; Blanco-Cabra, N.; Eguskiza, A.; Hortelao, A. C.; Torrents, E.; Sanchez, S. Drug-Free Enzyme-Based Bactericidal Nanomotors against Pathogenic Bacteria. *ACS Appl. Mater. Interfaces* **2021**, *13*, 14964−14973.
(14) Simmchen, J.; Baeza, A.; Miguel-Lopez, A.; Stanton, M. M.; Vallet-Regi, M.; Ruiz-Molina, D.; Sánchez, S. Dynamics of Novel Photoactive AgCl Microstars and Their Environmental Applications. *Chem. Commun.* **2017**, *3*, 65−71.
(15) Ma, E.; Wang, K.; Hu, Z.; Wang, H. Dual-Stimuli-Responsive CuS-Based Micromotors for Efficient Photo-Fenton Degradation of Antibiotics. *J. Colloid Interface Sci.* **2021**, *603*, 685−694.
(16) You, Y.; Xu, D.; Pan, X.; Ma, X. Self-Propelled Enzymatic Nanomotors for Enhancing Synergetic Photodynamic and Starvation Therapy by Self-Accelerated Cascade Reactions. *Appl. Mater. Today* **2019**, *16*, 508−517.
(17) Wu, J.; Ma, S.; Li, M.; Hu, X.; Jiao, N.; Tung, S.; Liu, L. Enzymatic/Magnetic Hybrid Micromotors for Synergistic Anticancer Therapy. *ACS Appl. Mater. Interfaces* **2021**, *13*, 31514−31526.
(18) Orozco, J.; Vilela, D.; Valdés-Ramírez, G.; Fedorak, Y.; Escarpa, A.; Vazquez-Duhalt, R.; Wang, J. Efficient Biocatalytic Degradation of Pollutants by Enzyme-Releasing Self-Propelled Motors. *Chem.—Eur. J.* **2014**, *20*, 2866−2871.
(19) Sattayasamitsathit, S.; Kaufmann, K.; Galarnyk, M.; Vazquez-Duhalt, R.; Wang, J. Dual-Enzyme Natural Motors Incorporating Decontamination and Propulsion Capabilities. *RSC Adv.* **2014**, *4*, 27565−27570.
(20) Orozco, J.; Mercante, L. A.; Pol, R.; Merkoçi, A. Graphene-Based Janus Micromotors for the Dynamic Removal of Pollutants. *J. Mater. Chem. A* **2016**, *4*, 3371−3378.
(21) Singh, V. V.; Jurado-Sánchez, B.; Sattayasamitsathit, S.; Orozco, J.; Li, J.; Galarnyk, M.; Fedorak, Y.; Wang, J. Multifunctional Silver-Exchanged Zeolite Micromotors for Catalytic Detoxification of Chemical and Biological Threats. *Adv. Funct. Mater.* **2015**, *25*, 2147−2155.
(22) Parmar, J.; Villa, K.; Vilela, D.; Sánchez, S. Platinum-Free Cobalt Ferrite Based Micromotors for Antibiotic Removal. *Appl. Mater. Today* **2017**, *9*, 605−611.
(23) Lu, A. X.; Liu, Y.; Oh, H.; Gargava, A.; Kendall, E.; Nie, Z.; DeVoe, D. L.; Raghavan, S. R. Catalytic Propulsion and Magnetic Steering of Soft, Patchy Microcapsules: Ability to Pick-up and Drop-off Microscale Cargo. *ACS Appl. Mater. Interfaces* **2016**, *8*, 15676−15683.
(24) Orozco, J.; Jurado-Sánchez, B.; Wagner, G.; Gao, W.; Vazquez-Duhalt, R.; Sattayasamitsathit, S.; Galarnyk, M.; Cortés, A.; Saintillan, D.; Wang, J. Bubble-Propelled Micromotors for Enhanced Transport of Passive Tracers. *Langmuir* **2014**, *30*, 5082−5087.
(25) Orozco, J.; Pan, G.; Sattayasamitsathit, S.; Galarnyk, M.; Wang, J. Micromotors to Capture and Destroy Anthrax Simulant Spores. *Analyst* **2015**, *140*, 1421−1427.
(26) Hwang, J.; Yang, H.-M.; Lee, K.-W.; Jung, Y.-I.; Lee, K. J.; Park, C. W. A Remotely Steerable Janus Micromotor Adsorbent for the Active Remediation of Cs-Contaminated Water. *J. Hazard. Mater.* **2019**, *369*, 416−422.
(27) Ma, X.; Sanchez, S. A Bio-Catalytically Driven Janus Mesoporous Silica Cluster Motor with Magnetic Guidance. *Chem. Commun.* **2015**, *51*, 5467−5470.
(28) Jurado-Sánchez, B.; Pacheco, M.; Rojo, J.; Escarpa, A. Magnetocatalytic Graphene Quantum Dots Janus Micromotors for Bacterial Endotoxin Detection. *Angew. Chem., Int. Ed.* **2017**, *56*, 6957−6961.
(29) Wu, Y.; Si, T.; Shao, J.; Wu, Z.; He, Q. Near-Infrared Light-Driven Janus Capsule Motors: Fabrication, Propulsion, and Simulation. *Nano Res.* **2016**, *9*, 3747−3756.
(30) de Ávila, B. E.-F.; Angsantikul, P.; Li, J.; Lopez-Ramirez, M. A.; Ramírez-Herrera, D. E.; Thamphiwatana, S.; Chen, C.; Delezuk, J.; Samakapiruk, R.; Ramez, V. Micromotor-Enabled Active Drug Delivery for in Vivo Treatment of Stomach Infection. *Nat. Commun.* **2017**, *8*, 272.
(31) Peng, F.; Men, Y.; Tu, Y.; Chen, Y.; Wilson, D. A. Nanomotor-Based Strategy for Enhanced Penetration across Vasculature Model. *Adv. Funct. Mater.* **2018**, *28*, 1706117.
(32) Tu, Y.; Peng, F.; White, P. B.; Wilson, D. A. Redox-sensitive Stomatocyte Nanomotors: Destruction and Drug Release in the Presence of Glutathione. *Angew. Chem., Int. Ed.* **2017**, *56*, 7620−7624.
(33) Guix, M.; Weiz, S. M.; Schmidt, O. G.; Medina-Sánchez, M. Self-Propelled Micro/Nanoparticle Motors. *Part. Part. Syst. Charact.* **2018**, *35*, 1700382.
(34) Habte, M. L.; Beyene, E. A. Biological Application and Disease of Oxidoreductase Enzymes. *Oxidoreductase*; IntechOpen, 2020.
(35) Alneyadi, A. H.; Rauf, M. A.; Ashraf, S. S. Oxidoreductases for the Remediation of Organic Pollutants in Water−a Critical Review. *Crit. Rev. Biotechnol.* **2018**, *38*, 971.
(36) Yang, J.; Li, W.; Ng, T. B.; Deng, X.; Lin, J.; Ye, X. Laccases: Production, Expression Regulation, and Applications in Pharmaceutical Biodegradation. *Front. Microbiol.* **2017**, *8*, 832.
(37) Li, M.; Huang, X.-R.; Guo, Y.; Shang, Y.-Z.; Liu, H.-L. A Novel Efficient Medium for Chromogenic Catalysis of Tetramethylbenzidine with Horseradish Peroxidase. *Chin. Chem. Lett.* **2017**, *28*, 1453−1459.
(38) Orozco, J.; Medlin, L. K. Electrochemical Performance of a DNA-Based Sensor Device for Detecting Toxic Algae. *Sens. Actuators, B* **2011**, *153*, 71−77.
(39) Cajigas, S.; Alzate, D.; Orozco, J. Gold Nanoparticle/DNA-Based Nanobioconjugate for Electrochemical Detection of Zika Virus. *Microchim. Acta* **2020**, *187*, 594.
(40) Orozco, J.; García-Gradilla, V.; D'Agostino, M.; Gao, W.; Cortés, A.; Wang, J. Artificial Enzyme-Powered Microfish for Water-Quality Testing. *ACS Nano* **2013**, *7*, 818−824.
(41) Kaushal, J.; Mehandia, S.; Singh, G.; Raina, A.; Arya, S. K. Catalase Enzyme: Application in Bioremediation and Food Industry. *Biocatal. Agric. Biotechnol.* **2018**, *16*, 192−199.
(42) Ma, X.; Sánchez, S. Bio-Catalytic Mesoporous Janus Nano-Motors Powered by Catalase Enzyme. *Tetrahedron* **2017**, *73*, 4883−4886.
(43) Sharifi, M.; Sohrabi, M. J.; Hosseinali, S. H.; Hasan, A.; Kani, P. H.; Talaei, A. J.; Karim, A. Y.; Nanakali, N. M. Q.; Salihi, A.; Aziz, F. M.; Yan, B.; Khan, R. H.; Saboury, A. A.; Falahati, M. Enzyme Immobilization onto the Nanomaterials: Application in Enzyme Stability and Prodrug-Activated Cancer Therapy. *Int. J. Biol. Macromol.* **2020**, *143*, 665−676.
(44) Neves-Petersen, M. T.; Klitgaard, S.; Carvalho, A. S. L.; Petersen, S. B.; Aires de Barros, M. R.; e Melo, E. P. Photophysics and Photochemistry of Horseradish Peroxidase A2 upon Ultraviolet Illumination. *Biophys. J.* **2007**, *92*, 2016−2027.
(45) Cacciari, R. D.; Reynoso, A.; Sosa, S.; Parodi, F.; Goldbaum, F. A.; Montejano, H. A.; Biasutti, M. A.; Reynoso, E. Effect of UVB Solar Irradiation on Laccase Enzyme: Evaluation of the Photooxidation Process and Its Impact over the Enzymatic Activity for Pollutants Bioremediation. *Amino Acids* **2020**, *52*, 925−939.
(46) Aubailly, M.; Haigle, J.; Giordani, A.; Morlière, P.; Santus, R. UV Photolysis of Catalase Revisited: A Spectral Study of Photolytic Intermediates. *J. Photochem. Photobiol., B* **2000**, *56*, 61−67.
(47) Lele, B. S.; Russell, A. J. Enhancing Enzyme Stability against TiO2-UV Induced Inactivation. *Biomacromolecules* **2005**, *6*, 475−482.
(48) Tiberio, G.; Muccioli, L.; Berardi, R.; Zannoni, C. How Does the Trans-Cis Photoisomerization of Azobenzene Take Place in Organic Solvents? *ChemPhysChem* **2010**, *11*, 1018.
(49) Pérez-Buitrago, S.; Mena-Giraldo, P.; Pinal, R.; Hoyos-Palacio, L. Azopolymer Based Nanoparticles for Phototriggered Drug Delivery. In *2019 41st Annual International Conference of the IEEE Engineering in Medicine and Biology Society (EMBC)*; IEEE, 2019; pp 1089−1092.
(50) Molla, M. R.; Rangadurai, P.; Antony, L.; Swaminathan, S.; de Pablo, J. J.; Thayumanavan, S. Dynamic Actuation of Glassy Polymersomes through Isomerization of a Single Azobenzene Unit at the Block Copolymer Interface. *Nat. Chem.* **2018**, *10*, 659−666.

https://doi.org/10.1021/acsami.1c14663
ACS Appl. Mater. Interfaces XXXX, XXX, XXX−XXX

(51) Mena-Giraldo, P.; Orozco, J. Polymeric Micro/Nanocarriers and Motors for Cargo Transport and Phototriggered Delivery. *Polymers* **2021**, *13*, 3920.
(52) BEYRİBEY, B.; Corbacioğlu, B.; Altin, Z. Synthesis of Platinum Particles from H2PtCl6 with Hydrazine as Reducing Agent. *Gazi Univ. J. Sci.* **2009**, *22*, 351−357.
(53) Tonigold, M.; Simon, J.; Estupiñán, D.; Kokkinopoulou, M.; Reinholz, J.; Kintzel, U.; Kaltbeitzel, A.; Renz, P.; Domogalla, M. P.; Steinbrink, K.; Lieberwirth, I.; Crespy, D.; Landfester, K.; Mailänder, V. Pre-Adsorption of Antibodies Enables Targeting of Nanocarriers despite a Biomolecular Corona. *Nat. Nanotechnol.* **2018**, *13*, 862−869.
(54) Meng, L.; Huang, W.; Wang, D.; Huang, X.; Zhu, X.; Yan, D. Chitosan-Based Nanocarriers with PH and Light Dual Response for Anticancer Drug Delivery. *Biomacromolecules* **2013**, *14*, 2601−2610.
(55) Mena-Giraldo, P.; Pérez-Buitrago, S.; Londoño-Berrío, M.; Ortiz-Trujillo, I. C.; Hoyos-Palacio, L. M.; Orozco, J. Photosensitive Nanocarriers for Specific Delivery of Cargo into Cells. *Sci. Rep.* **2020**, *10*, 2110−12.
(56) He, M.; Han, B.; Jiang, Z.; Yang, Y.; Peng, Y.; Liu, W. Synthesis of a Chitosan-Based Photo-Sensitive Hydrogel and Its Biocompatibility and Biodegradability. *Carbohydr. Polym.* **2017**, *166*, 228−235.
(57) Ma, G.; Qian, B.; Yang, J.; Hu, C.; Nie, J. Synthesis and Properties of Photosensitive Chitosan Derivatives (1). *Int. J. Biol. Macromol.* **2010**, *46*, 558−561.
(58) Wu, S.; Zeng, F.; Zhu, H.; Tong, Z. Energy and Electron Transfers in Photosensitive Chitosan. *J. Am. Chem. Soc.* **2005**, *127*, 2048−2049.
(59) Cheng, N.; Cao, X. Photosensitive Chitosan to Control Cell Attachment. *J. Colloid Interface Sci.* **2011**, *361*, 71−78.
(60) Gür, S. D.; İdil, N.; Aksöz, N. Optimization of Enzyme Co-Immobilization with Sodium Alginate and Glutaraldehyde-Activated Chitosan Beads. *Appl. Biochem. Biotechnol.* **2018**, *184*, 538−552.
(61) Wei, W.; Wang, L.-Y.; Yuan, L.; Wei, Q.; Yang, X.-D.; Su, Z.-G.; Ma, G.-H. Preparation and Application of Novel Microspheres Possessing Autofluorescent Properties. *Adv. Funct. Mater.* **2007**, *17*, 3153−3158.
(62) Wang, K.; Yuan, X.; Guo, Z.; Xu, J.; Chen, Y. Red Emissive Cross-Linked Chitosan and Their Nanoparticles for Imaging the Nucleoli of Living Cells. *Carbohydr. Polym.* **2014**, *102*, 699−707.
(63) Li, Q.-W.; Su, Y.-X.; Zou, H.; Chen, Y.-Y.; Zhou, L.; Hou, X.-H.; Liu, N.; Wu, Z.-Q. Self-Assembly and Fluorescence Emission of UV-Responsive Azobenzene-Containing Helical Poly (Phenyl Isocyanide) Copolymers. *Polym. Chem.* **2020**, *11*, 6029−6036.
(64) Ishikawa, T.; Noro, T.; Shoda, T. Theoretical Study on the Photoisomerization of Azobenzene. *J. Chem. Phys.* **2001**, *115*, 7503−7512.
(65) Han, M.; Hara, M. Intense Fluorescence from Light-Driven Self-Assembled Aggregates of Nonionic Azobenzene Derivative. *J. Am. Chem. Soc.* **2005**, *127*, 10951−10955.
(66) Wu, J.; Xu, B.; Liu, Z.; Yao, Y.; Zhuang, Q.; Lin, S. The Synthesis, Self-Assembly and PH-Responsive Fluorescence Enhancement of an Alternating Amphiphilic Copolymer with Azobenzene Pendants. *Polym. Chem.* **2019**, *10*, 4025−4030.
(67) Yang, J.; Li, J.; Ng, D. H. L.; Yang, P.; Yang, W.; Liu, Y. Micromotor-Assisted Highly Efficient Fenton Catalysis by a Laccase/Fe-BTC-NiFe 2 O 4 Nanozyme Hybrid with a 3D Hierarchical Structure. *Environ. Sci.: Nano* **2020**, *7*, 2573−2583.
(68) Sojitra, U. V.; Nadar, S. S.; Rathod, V. K. Immobilization of Pectinase onto Chitosan Magnetic Nanoparticles by Macromolecular Cross-Linker. *Carbohydr. Polym.* **2017**, *157*, 677−685.
(69) García-Torres, J.; Serrà, A.; Tierno, P.; Alcobé, X.; Vallés, E. Magnetic Propulsion of Recyclable Catalytic Nanocleaners for Pollutant Degradation. *ACS Appl. Mater. Interfaces* **2017**, *9*, 23859−23868.
(70) Báez, D. F.; Ramos, G.; Corvalán, A.; Cordero, M. L.; Bollo, S.; Kogan, M. J. Effects of Preparation on Catalytic, Magnetic and Hybrid Micromotors on Their Functional Features and Application in Gastric Cancer Biomarker Detection. *Sens. Actuators, B* **2020**, *310*, 127843.
(71) Campuzano, S.; Esteban-Fernández de Ávila, B.; Yáñez-Sedeño, P.; Pingarrón, J. M.; Wang, J. Nano/Microvehicles for Efficient Delivery and (Bio) Sensing at the Cellular Level. *Chem. Sci.* **2017**, *8*, 6750−6763.
(72) Bilal, M.; Jing, Z.; Zhao, Y.; Iqbal, H. M. N. Immobilization of Fungal Laccase on Glutaraldehyde Cross-Linked Chitosan Beads and Its Bio-Catalytic Potential to Degrade Bisphenol A. *Biocatal. Agric. Biotechnol.* **2019**, *19*, 101174.
(73) Belho, K.; Ambasht, P. K. Immobilization of Phytase from Rice Bean (Vigna Umbellata Thunb.) on Glutaraldehyde Activated Chitosan Microspheres. *J. Sci. Res.* **2021**, *65*, 111−119.
(74) Verma, M. L.; Kumar, S.; Das, A.; Randhawa, J. S.; Chamundeeswari, M. Chitin and Chitosan-Based Support Materials for Enzyme Immobilization and Biotechnological Applications. *Environ. Chem. Lett.* **2020**, *18*, 315−323.
(75) Grotjohann, N.; Janning, A.; Eising, R. In VitroPhotoinactivation of Catalase Isoforms from Cotyledons of Sunflower (Helianthus AnnuusL.). *Arch. Biochem. Biophys.* **1997**, *346*, 208−218.
(76) Shivaramu, P. D.; Patil, A.; Murthy, M.; Tubaki, S.; Shastri, M.; Manjunath, S.; Gangaraju, V.; Rangappa, D. Magnetic Substrate Supported ZnO-CuO Nanocomposite as Reusable Photo Catalyst for the Degradation of Organic Dye. *Mater. Today: Proc.* **2017**, *4*, 12314−12320.
(77) Han, W.; Zhu, W.; Zhang, P.; Zhang, Y.; Li, L. Photocatalytic Degradation of Phenols in Aqueous Solution under Irradiation of 254 and 185 Nm UV Light. *Catal. Today* **2004**, *90*, 319−324.
(78) Martins, D.; English, A. M. Catalase Activity Is Stimulated by H_2O_2 in Rich Culture Medium and Is Required for H2O2 Resistance and Adaptation in Yeast. *Redox Biol.* **2014**, *2*, 308−313.

https://doi.org/10.1021/acsami.1c14663
ACS Appl. Mater. Interfaces XXXX, XXX, XXX−XXX